Aerosol Science and Technology
Publication details, including instructions for authors and subscription information:
http://www.tandfonline.com/loi/uast20

A New Cross-Flow Tube Bundle Heat Exchanger with Staggered Hot and Cold Tubes for Thermophoretic Deposition of Submicron Aerosol Particles

Chih-Liang Chien [a] , Shih-Hsuan Huang [a] & Chuen-Jinn Tsai [a]
[a] Institute of Environmental Engineering, National Chiao Tung University , Hsin Chu, Taiwan
Published online: 05 Oct 2009.

To cite this article: Chih-Liang Chien , Shih-Hsuan Huang & Chuen-Jinn Tsai (2009) A New Cross-Flow Tube Bundle Heat Exchanger with Staggered Hot and Cold Tubes for Thermophoretic Deposition of Submicron Aerosol Particles, Aerosol Science and Technology, 43:12, 1153-1163, DOI: 10.1080/02786820903242011

To link to this article: http://dx.doi.org/10.1080/02786820903242011

Aerosol Science and Technology, 43:1153–1163, 2009

ISSN: 0278-6826 print / 1521-7388 online
DOI: 10.1080/02786820903242011

A New Cross-Flow Tube Bundle Heat Exchanger with Staggered Hot and Cold Tubes for Thermophoretic Deposition of Submicron Aerosol Particles

Chih-Liang Chien, Shih-Hsuan Huang, and Chuen-Jinn Tsai
Institute of Environmental Engineering, National Chiao Tung University, Hsin Chu, Taiwan

A new tube cross-flow bundle heat exchanger has been designed and tested for thermophoretic deposition of submicron aerosol particles. The present design has five columns of hot and cold square tubes, respectively, arranged in a staggered manner to maintain a nearly constant temperature gradient in the direction of the aerosol flow. Each column has four tubes of 4 mm × 4 mm in cross section and the gap between the tube surfaces is 0.5 mm. The precipitator was tested experimentally using monodisperse NaCl test particles ranging from 38 to 397 nm in diameter at the aerosol flow rate of 0.6 and 1.2 L/min, respectively, at different temperature gradients. Results showed that the thermophoretic deposition efficiency increased with decreasing aerosol flow rate and increasing temperature gradient with the maximum thermophoretic deposition efficiency occurred at the aerosol flow rate of 0.6 L/min. The effect of inlet temperature of the aerosol flow on the efficiency was also tested and showed increasing inlet temperature increased the deposition efficiency. Numerical simulation was further conducted to validate the experimental data and good agreement was obtained. An empirical equation was also validated to facilitate the design and scale-up of the precipitator.

INTRODUCTION

Thermophoresis is a physical phenomenon in which aerosol particles move toward the direction of decreasing temperature when subjected to a thermal gradient. Thermophoretic precipitator can be used for aerosol sampling (Maynard 1995; Bang et al. 2003; Lorenzo et al. 2007; Wen et al. 2007) as well as submicron particle control (Shi and Harrison 2001; Messerer et al. 2003). Extensive literature has been published for thermophoretic precipitation in pipe flow (Batchelor and Shen 1985; Montassier et al. 1990, 1991; Stratmann et al. 1994; Chang et al. 1995; He and Ahmadi 1998; Romay et al. 1998; Lin and Tsai 2003; Lin et al. 2004; Tsai et al. 2004; Lee et al. 2006; Lin et al. 2008), in flow between parallel plates (Maynard 1995; Tsai and Lu 1995; Gonzalez et al. 2005), and in tube bundle heat exchanger (Messerer et al. 2004; Messerer et al. 2007). The computational fluid dynamics (CFD) codes was further used to investigate aerosol dynamics (Stratmann and Whitby 1989; Pyykönen and Jokiniemi 2000), thermophoretic deposition in tube flow (Housiadas et al. 2001; Housiadas and Drossinos 2003; Housiadas and Drossinos 2005; Munoz-Bueno et al. 2005) and in thermophoretic precipitator (Gonzalez et al. 2005).

Heat exchangers made from tube bundles are widely used and found in numerous industrial applications. Messerer et al. (2004) first proposed a miniature pipe bundle heat exchanger for thermophoretic deposition of ultrafine aerosol particles at high flow rate. Miniature tubes with an inner diameter of 0.99 mm and an outer diameter of 1.59 mm were used mainly to maintain small gaps between the surfaces of the tubes so that effective thermophoretic deposition could be achieved. The same heat exchanger system was further operated in the exhaust gas lines of two wood-fired heating appliances and particle deposition efficiency up to 95% was achieved (Messerer et al. 2007). However, thermal gradient decreases exponentially with the increasing downstream distance along the flow direction and limits the effective thermophoretic deposition region near the entry of the tubes (Lin et al. 2004), and only the first few centimeters of the heat exchanger was found to be effective for thermophoretic deposition (Messerer et al. 2004).

In order to eliminate this limitation, a cross-flow type tube bundle heat exchanger was designed in this study. The exchanger has 5 columns of cold square tubes (cross section: 4 × 4 mm) arranged in a staggered manner with another 5 columns of hot square tubes of the same cross section to keep the temperature gradient constant in the flow direction of the precipitator. The flow channels in the square tubes are cylindrical having a diameter of 2 mm. The square tubes are used for easy adjustment of a small and constant gap between the hot and cold surfaces without the need to use the miniature circular tube design as in Messerer et al. (2004). In this study, a 2-D numerical simulation was further conducted to obtain simulated particle deposition efficiency for the comparison with the experimental results. An empirical equation of the plate-to-plate thermophoretic

Recieved 23 March 2009; accepted 4 August 2009.
The financial support of this work by the Taiwan National Science Council (NSC92-2211-E-009-037) is gratefully acknowledged.
Address correspondence to Chuen-Jinn Tsai, Institute of Environmental Engineering, National Chiao Tung University, No. 1001, University Road, Hsin Chu, 300 Taiwan. E-mail: cjtsai@mail.nctu.edu.tw

precipitator for the thermophoretic deposition efficiency derived by Tsai and Lu (1995) was also validated to facilitate the design and scale-up of the precipitator.

New Tube Bundle Heat Exchanger AS Thermophoretic Precipitator

Figures 1a and b show the cross-sectional and exploded views of the new tube bundle heat exchanger used as the thermophoretic precipitator, respectively. The precipitator has a rectangular frame (64.5 × 20 × 20 mm) which contains a hot-side heat exchanger, and a cold-side heat exchanger, each has five tube columns. Each column of four hot tubes is staggered with the other column of four cold tubes. Asbestos spacers are placed between the heat exchangers and the housing to reduce conductive heat transfer. The gap between the tube surfaces is 0.5 mm. The aerosol flow first passes through the first column of the four hot tubes followed by the first column of the four cold tubes. Then the aerosol flow passes through the other columns of the hot and cold tubes alternately again in the direction of the aerosol flow. Thermophoretic precipitation occurs in the vertical gaps where the temperature gradient exists between the hot and cold tubes.

Figures 1c and d show the first column (section A-A) of four hot tubes, in which hot silicon oil flows, and the first column (section B-B) of four cold tubes in which cold water flows, respectively. The hot tubes are heated by circulating silicon oil at different temperatures of 423, 443, and 473 K, respectively, while the cold tubes are cooled by circulating water at room temperature. Forced convection by hot silicon oil and cold water is necessary for establishing a temperature difference between the cold and hot tubes to increase the thermophoretic particle deposition efficiency (Tsai and Lu 1995).

METHODS

Experimental Method

The experimental setup is shown in Figure 2. Monodisperse NaCl particles ranging from 38 to 397 nm in diameter were generated by the atomization and electrostatic classification technique. The polydisperse aerosol was first generated by atomizing 0.1% w/v aqueous solution of NaCl using a constant output atomizer (TSI model 3076) and passed through a silica gel diffusion dryer. Then it was mixed with clean dry air in a mixing tank. After being mixed, the aerosol was neutralized by a TSI 3077 electrostatic charge neutralizer before being introduced into a TSI 3081 Long DMA (differential mobility analyzer) where a high voltage was applied to select monodisperse test particles. The monodisperse aerosol from the DMA was neutralized again before being introduced into the precipitator. For the experiment involving higher temperature of the inlet air flow than the room temperature, the aerosol stream was passed through a stainless steel tube wrapped in a heating tape and was heated to a desired temperature. The flow rate of the sheath air and polydisperse aerosol stream of the DMA was kept constant at 5 and 0.5 L/min, respectively, throughout the experiment.

Two J-type thermocouples installed at the inlet and outlet of the precipitator were used to monitor the temperature of the aerosol stream. The other four thermocouples were attached on the first two columns (the location of thermocouple: point a and b) and the last two columns (the location of thermocouple: point c and d) to measure the surface temperatures, as shown in Figure 1a. The average temperature difference was calculated as the temperature difference between the hot and cold tubes. The flow rate of the aerosol flow was set by a mass flow controller (calibrated at standard conditions of 298 K, 1 atm, MKS Instruments, Inc. model 1179A) located downstream of the precipitator. The aerosol number concentrations at the inlet and outlet of the precipitator were measured using a TSI 3022 condensation particle counter (CPC) with a sampling flow rate of 0.3 L/min.

Particle deposition in the new thermophoretic precipitator was tested at two aerosol flow rates of 0.6 and 1.2 L/min, respectively, and at three temperature differences by adjusting the temperature of the hot silicon oil bath to be 423, 443, and 473 K while maintaining the cold water temperature at 300 K. Measured temperature data in the precipitator are listed in Table 1. For example, when the hot silicon oil bath was kept at 423, 443, and 473 K, respectively, at the aerosol flow rate of 0.6 L/min, the corresponding surface temperature of the first column of the four hot tubes at the point "a" was measured to be 346.5, 360.0, and 391.1 K, respectively. Or the temperature difference between the hot and cold tube surfaces was 45.5, 58.9, and 88.6 K, respectively. At both flow rates, the surface temperature of the last column of the hot tubes is higher than that of the first column of the hot tubes. The temperature difference between the hot and cold tubes remains high in the direction of the flow. Therefore, it is to be expected that the thermophoretic deposition will be effective throughout the whole thermophoretic precipitator.

The particle deposition efficiency was determined from the particle concentrations measured at the inlet and outlet of the thermophoretic precipitator. The deposition efficiency, η, can be calculated as

$$\eta = 1 - \frac{N_o}{N_i} \qquad [1]$$

where N_i and N_o are the particle concentrations at the inlet and outlet of the new tube bundle thermophoretic precipitator, respectively. The total particle deposition efficiency, η_{tot}, includes the isothermal contribution, η_{iso}, caused by particle deposition due to diffusion and interception under isothermal flow conditions, and the thermophoretic contribution, η_{th}. In the experiment, the isothermal contribution was first determined under isothermal conditions when the thermal gradient between

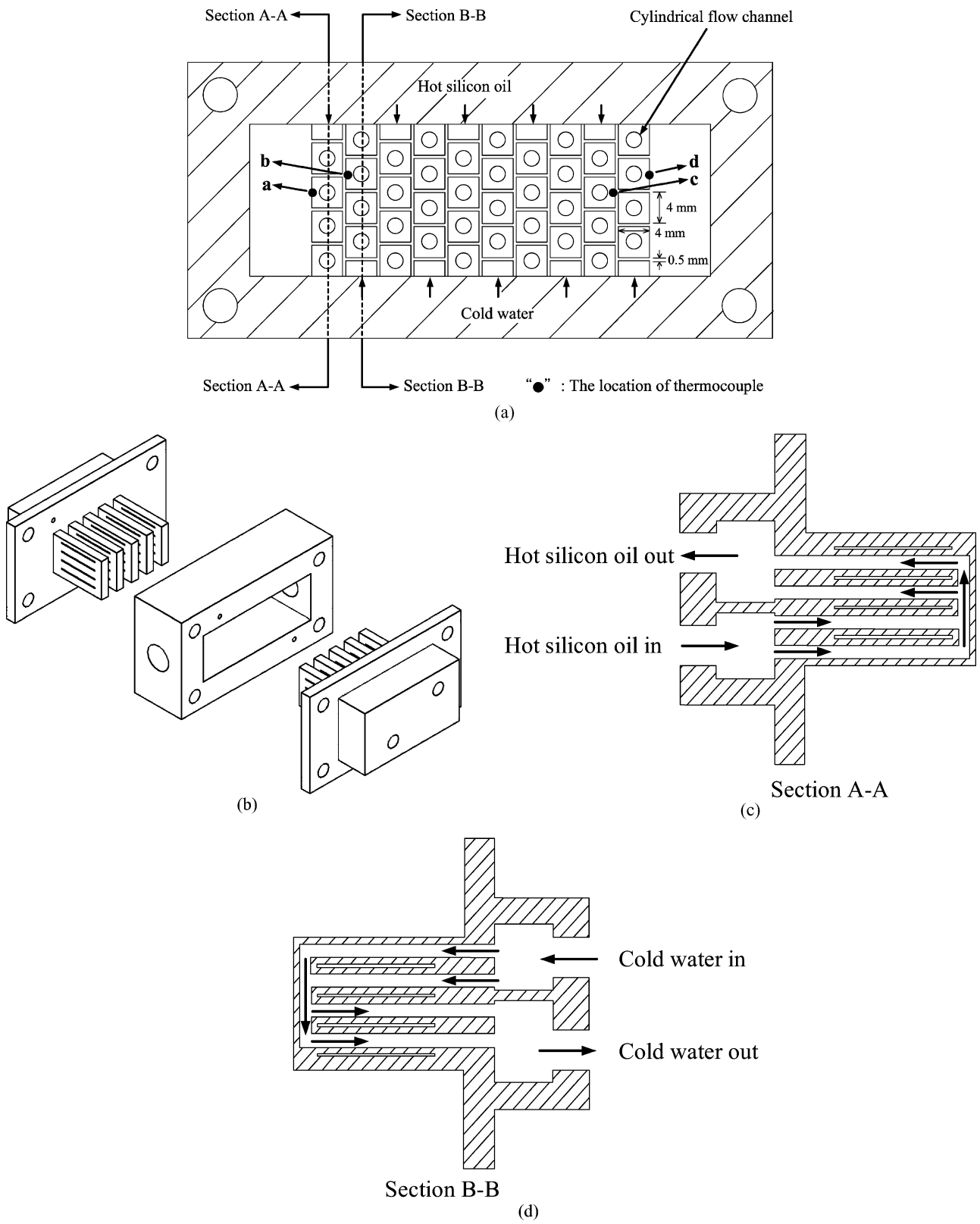

FIG. 1. Schematic diagram of the present thermophoretic precipitator made of tube bundle heat exchanger. (a) Cross-sectional view. (b) Exploded view. (c) The first column of the four hot square tubes (section A-A). (d) The first column of the four cold square tubes (section B-B).

TABLE 1
Simulated average flow velocity, pressure drop, and measured temperature data in the tube bundle heat exchanger

T_{hot}*, K	Q, L/min	Average flow velocity, m/s	Pressure drop, Pa	Temperature, K						
				T_{in}	T_{out}	Point "a"	Point "b"	Point "c"	Point "d"	ΔT**
423	0.6	0.5	156.6	302.4	303.4	346.5	306.0	351.5	301.0	45.5
	1.2	1.0	395.9	302.1	303.4	343.5	306.5	350.1	301.1	43
443	0.6	0.5	163.8	299.9	302.2	360.0	309.0	367.9	301.1	58.9
	1.2	1.1	411.9	300.3	302.8	357.7	309.4	366.7	301.3	56.9
473	0.6	0.5	175.9	299.8	299.6	391.1	311.2	397.8	300.5	88.6
	1.2	1.1	437.5	299.9	301.3	387.8	311.7	395.1	300.2	85.5

*Cold water temperature (T_{cold}) was kept at 300 K.
**The average temperature difference was calculated as the temperature difference between the hot and cold tubes.

the hot and cold tubes was zero. The experimental isothermal deposition efficiency without any thermal gradient is shown in Figure 3 at the aerosol flow rate of 0.6 L/min, which indicates that the isothermal contribution caused by diffusional deposition cannot be neglected because of the numerous flow bendings throughout the whole thermophoretic precipitator and the small gaps. The experimental thermophoretic deposition efficiency, η_{th}, was calculated as (Tsai and Lu 1995; Messerer et al. 2003, 2004):

$$\eta_{th} = \frac{\eta_{tot} - \eta_{iso}}{1 - \eta_{iso}} \quad [2]$$

In the present study, data points with error bars in the figures represent the arithmetic mean ± one standard deviation of 3 repeated measurements, while each measurement consisted of 10 readings.

Numerical Method

In order to further understand the temperature field and deposition efficiency of the present precipitator, a 2-D numerical simulation was conducted in this study. The governing equations are Navier-Stokes, continuity and energy equations. Steady-state laminar incompressible flow was assumed. The Navier-Stokes, continuity, and energy equations were solved by using the STAR-CD 3.22 code (CD-adapco Japan Co., LTD) which is based on the finite volume discretization method. The pressure-velocity linkage was solved by the SIMPLE (semi-implicit method for pressure linked equation) algorithm (Patankar 1980).

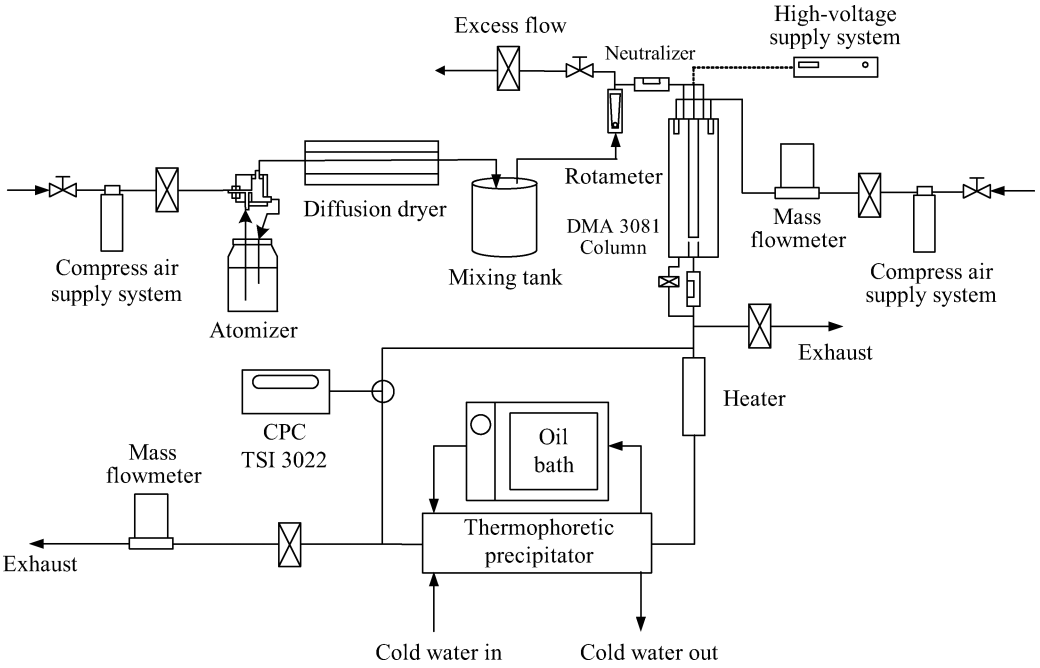

FIG. 2. Schematic diagram of the experimental setup.

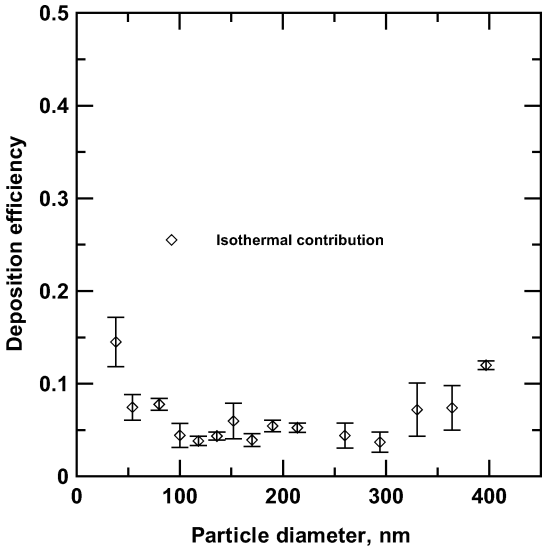

FIG. 3. Experimental isothermal deposition efficiency without any thermal gradient, aerosol flow rate = 0.6 L/min.

The UD (upwind differencing) and CD (central differencing) schemes were used for the space discretization method of the flow velocity and density, respectively. Hexahedral cells, which allowed for finer grid spacing near the wall, were generated by an automatic mesh generation tool, TrueGrid (version 2.1.0, XYZ Scientific Applications, Inc.). The total number of grids used is 300,000 in the calculation domain. The average grid size is around 30 μm with the smallest size of 0.9 μm assigned near the surfaces of the tubes. It was found that increasing the number of grids to 600,000 only resulted in a less than 1% difference in the thermophoretic deposition efficiency. Therefore, a fixed grid number of 300,000 was used for the calculation in this study. The convergence criterion of the flow field was set at 10^{-8} for the summation of the residuals.

Figure 4 shows the calculation domain of the numerical simulation. Bold lines represent the effective deposition length on the vertical surfaces of the cold tubes where particles deposit due to thermophoresis. In the simulation, the inlet region of the calculation domain, which was extended 10 mm from the entry of the thermophoretic precipitator, was set as the inlet boundary assuming a uniform velocity profile. To avoid the backward recirculation flow, the outlet region of the calculation domain was further extended 40 mm and 100 mm from the exit of the thermophoretic precipitator at the flow rate of 0.6 and 1.2 L/min, respectively. The surface temperature of the tubes was assigned based on the average temperature measured in this study. The upper symmetrical line was assumed to be the centerlines of the cold tubes while the bottom symmetrical line was assumed to be the centerline of the hot tubes in the longitudinal direction. The flow field was computed without using any periodical boundary conditions or repeated sections similar to Wang et al. (2000) and El-Shaboury et al. (2005).

After the flow field was obtained, the particle concentration field was calculated numerically by solving the following particle convection-diffusion equation:

$$\nabla \cdot \left(\vec{u}\, N\right) = \nabla \cdot (D \nabla \cdot N) - \nabla \cdot \left(\vec{V}_{th} N\right) \qquad [3]$$

where $\vec{V}_{th}$ is the particle thermophoretic velocity defined as:

$$\vec{V}_{th} = -\frac{\nu K_{th}}{T} \vec{\nabla} T \qquad [4]$$

The thermophoretic coefficient, K_{th}, is defined as (Talbot et al. 1980):

$$K_{th} = \frac{2C_S C}{(1 + 3C_m(2\lambda/d_p))} \times \left(\frac{k_g/k_p + C_t(2\lambda/d_p)}{1 + 2(k_g/k_p) + 2C_t(2\lambda/d_p)} \right) \qquad [5]$$

For accommodation, the reasonable values of C_m, C_s, and C_t are 1.14, 1.17, and 1.28, respectively (Talbot et al. 1980; Montassier et al. 1991).

In Equation (3), the boundary condition at the wall was assumed to be perfect absorption. Brownian diffusion was included and the current simulated isothermal deposition efficiency without any thermal gradient was found to be less 3% for particles from 38–100 nm in diameter. The numerical results of the thermophoretic deposition efficiency were calculated based on Equation (2) for comparison with the experimental data.

Theoretical Formulation of the Thermophoretic Deposition Efficiency

Under laminar flow condition, the thermophoretic deposition efficiency in a plate-to-plate thermophoretic precipitator can be calculated as (Tsai and Lu 1995; Messerer et al. 2003, 2004):

$$\eta_{th} = \frac{\left|\vec{V}_{th}\right| L}{v_{x,0} H} = K_{th} \frac{L \mu_{g,0} \Delta T}{\rho_{g,0} v_{x,0} H^2 T} \qquad [6]$$

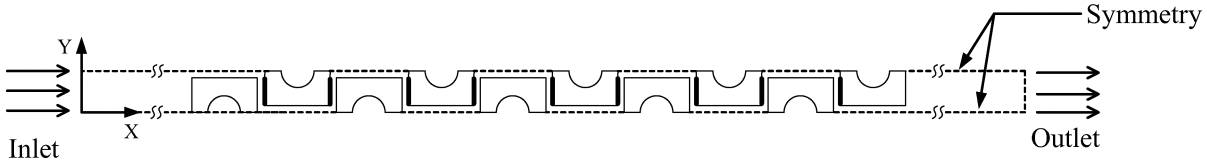

FIG. 4. Calculation domain of the numerical simulation. Bold lines represent the effective thermophoretic deposition length on the vertical gaps between the hot and cold tubes.

where H and ΔT are the gap and temperature difference between the plates, respectively. L is the length of thermophoretic deposition area. T, $\mu_{g,0}$, $\rho_{g,0}$, and $v_{x,0}$ are mean air temperature, dynamic viscosity, air density, and axial air flow velocity, respectively. Equation (6) is based on the assumption of a linear temperature profile and constant heat flux across the rectangular flow channel.

In this study, H is 0.5 mm, and L is the total effective deposition length on the vertical gaps between the hot and cold tubes. Mean air temperature, T, was calculated as the mean of the simulated air temperatures before the second column of the hot tubes and after the second last column of the cold tubes. This mean air temperature is more representative than that calculated from the inlet and outlet temperatures as the air flow is heated and cooled periodically in between the hot and cold tubes. Equation (6) will be validated by the experimental data to facilitate the design of the precipitator.

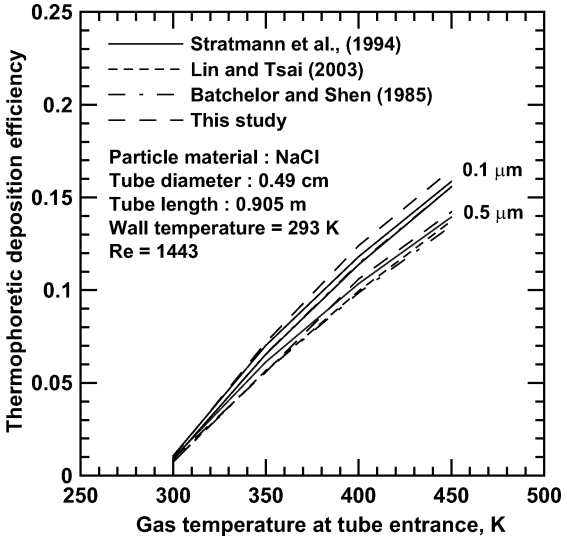

FIG. 5. Comparison of theoretical deposition efficiency with previous studies in laminar tube flow.

RESULTS AND DISCUSSIONS

Validation of the Simulation Method

The present simulation was validated by reproducing solutions for the benchmark problem in which the geometric configuration is similar to the design of the cross-flow tube bundle thermophoretic precipitator of this study. For the flow across a bundle of staggered tubes (O.D. = 16.4 mm, longitudinal pitch = 34.3 mm, transverse pitch = 31.3 mm) where seven rows of tubes are aligned in the air flow direction and each row has eight tubes, the calculated Nusselt number of the present simulation is 87.58, which is very close to 87.9 from the theoretical study of Incropera and DeWitt (2002) and 88.3 from the analytical solution of Khan et al. (2006). Details of parameters used to solve the problem of staggered tube bundle are described in Incropera and DeWitt (2002).

The simulated thermophoretic deposition efficiency in laminar tube flow of the present study was further compared with previous studies at the flow rate of 5 L/min for a long tube (I.D. = 0.0049 mm, length = 0.905 m). The simulated thermophoretic deposition efficiency in laminar tube flow shown in Figure 5 illustrates that the present numerical results are in good agreement with the predictions of Batchelor and Shen (1985), Stratmann et al. (1994), and Lin and Tsai (2003) with the deviation smaller than 2%. It can be seen that the thermophoretic deposition efficiency increases with an increasing inlet air flow temperature and decreasing particle size. Hence, these comparisons demonstrate that the present numerical simulation is accurate.

Thermophoretic Deposition Efficiency of the Present Thermophoretic precipitator

For the traditional thermophoretic precipitator, most of heat transfer occurs near the entry where the temperature gradient is high but decreases very quickly with the increasing distance from the entry of the precipitator. Figures 6a–d show the temperature field of the new thermophoretic precipitator when the hot silicon oil temperature is 423 K and 473 K at the flow rate of 0.6 L/min, respectively. Similar periodic temperature profiles are observed (figures not shown) for the other hot silicon oil temperatures of 443 K. That is, uniform temperature gradient and particle deposition on the vertical surfaces of the cold tubes are achieved along the precipitator and the overall thermophoretic deposition efficiency is expected to be high.

Figure 7 shows the particle concentration field of the new thermophoretic precipitator near the first two to five columns of tube bundles when the hot silicon oil temperature is 473 K at the flow rate of 0.6 L/min. Mass fraction of the initial particle concentration in the inlet air flow is 10^{-4} and particle diameter is 38 nm. The particle concentration contours shown in Figure 7 indicate particle concentration is gradually decreased as the aerosol flow passes through the bundles and the precipitator remains effective in the whole axial direction. This is in contrast to the sharp decrease of particle concentration in the entry of the traditional heat exchanger.

Figure 8 shows an example of the particle number distributions before and after the thermophoretic precipitator when the temperature difference between the hot and cold tubes is 45.5 K at the inlet aerosol flow rate of 0.6 L/min. The number concentration was seen to reduce very much after the precipitator.

The simulated average velocity and pressure drop of the air flow across the thermophoretic precipitator are listed Table 1. The average flow velocity is found to be 0.5 and 1.1 m/s at the flow rate of 0.6 and 1.2 L/min, respectively. The pressure drop increases with the increasing aerosol flow rate but remains small at three temperature differences.

The experimental, simulated and theoretical thermophoretic deposition efficiencies at three temperature differences are

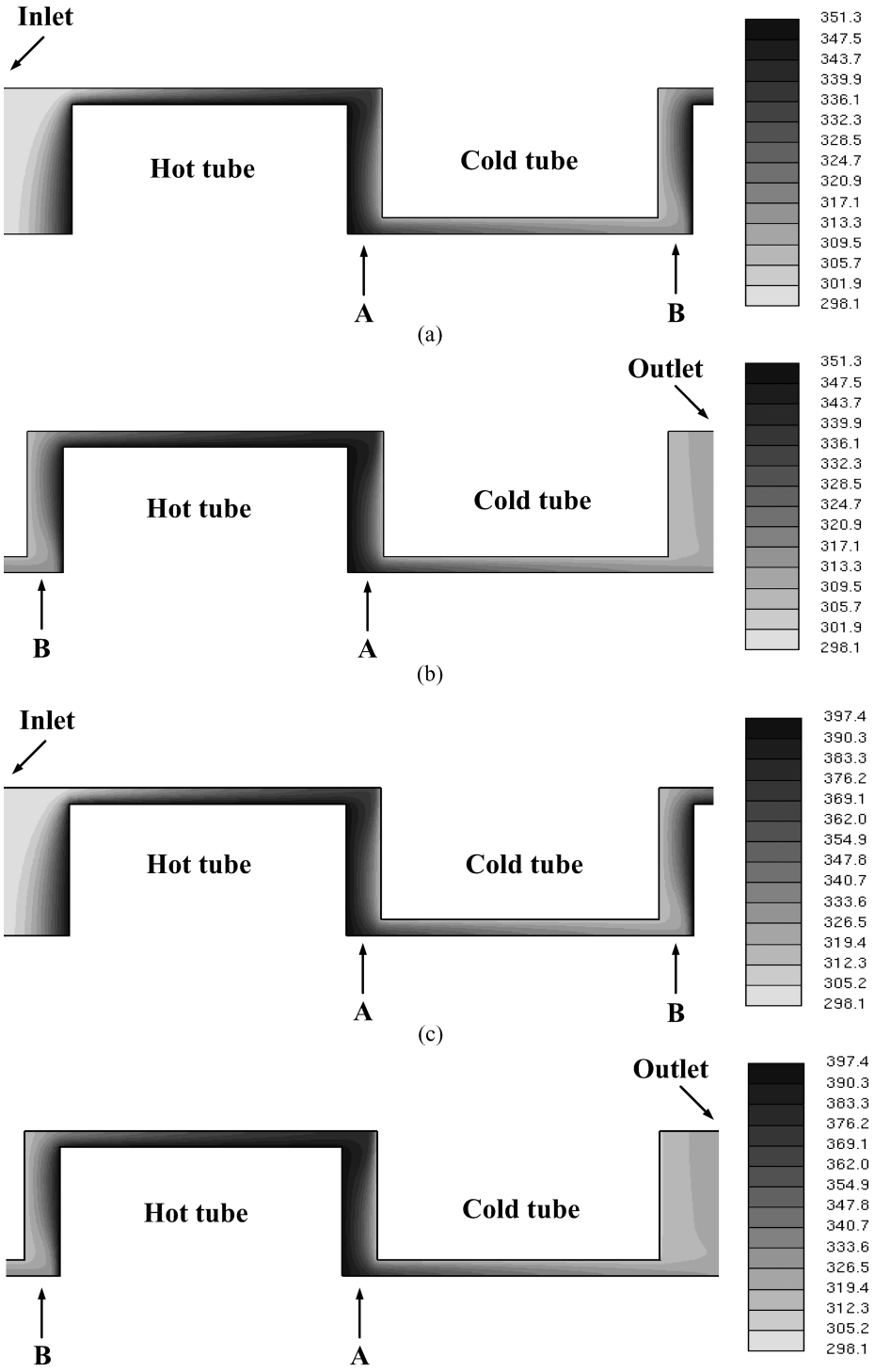

FIG. 6. Temperature field of the new thermophoretic precipitator at the flow rate of 0.6 L/min. (a) Near the first two columns of tube bundles, $T_{hot} = 423$ K. (b) Near the last two columns of tube bundles, $T_{hot} = 423$ K. (c) Near the first two columns of tube bundles, $T_{hot} = 473$ K. (d) Near the last two columns of tube bundles, $T_{hot} = 473$ K.

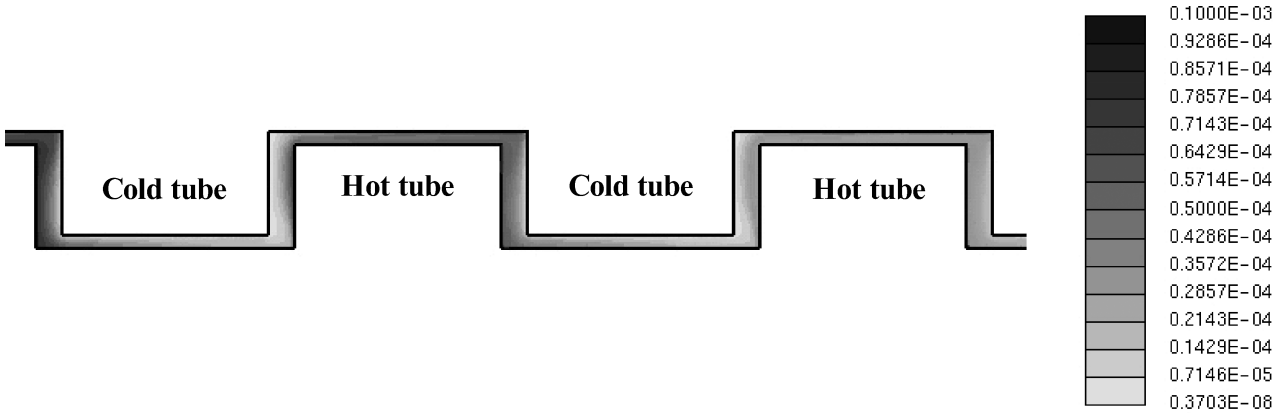

FIG. 7. Particle concentration field of the new thermophoretic precipitator near the first two to five columns of tube bundles when the hot silicon oil temperature is 473 K at the flow rate of 0.6 L/min. Mass fraction of the initial particle concentration in the inlet air flow is 10^{-4} and particle diameter is 38 nm.

plotted versus particle diameter in Figure 9, when the inlet air flow temperature is 298 K at the flow rate of 0.6 L/min. As shown in the figure, the experimental thermophoretic deposition efficiency is 59.3–63.4, 69.6–79.2, and 82.6–92.3% when the temperature difference is 45.5, 58.9, and 88.6 K, respectively. The thermophoretic deposition efficiency is increased with increasing temperature differences between the hot and cold tubes at a given air flow rate. The current thermophoretic precipitator has good particle deposition efficiencies up to 92%. The simulated thermophoretic deposition efficiency, which is 66.8–68.4, 79.8–81.4, and 89.8–92.3% when the temperature difference is 45.5, 58.9, and 88.6 K, respectively, is nearly independent of particle size at three temperature differences. The maximum deviation of the present simulation from the experimental data is 10.2%.

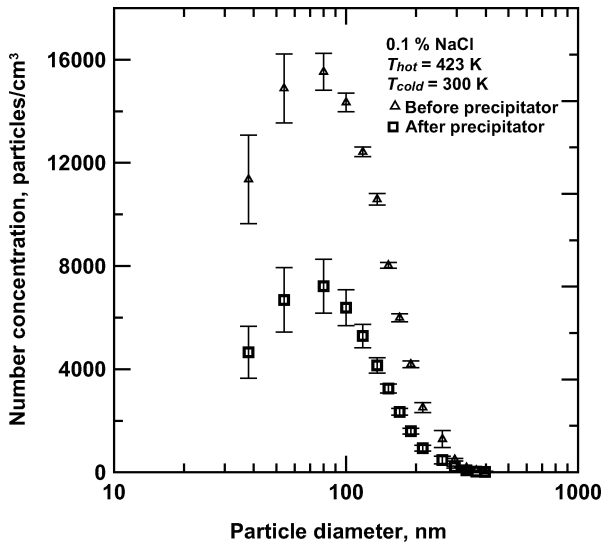

FIG. 8. A typical number concentration distribution of test particles before and after the new thermophoretic precipitator. Temperature difference: 45.5 K, aerosol flow rate: 0.6 L/min. Error bars represent the standard deviation of repeated measurements.

The theoretical thermophoretic deposition efficiency is found to be 57.4–66.8, 75.2–87.4, and 100% when the temperature difference is 45.5, 58.9, and 88.6 K, respectively. The theoretical thermophoretic deposition efficiencies are within a reasonable range of the experimental data but a discrepancy exists. The discrepancy between the experimental themophoretic efficiencies and numerical or theoretical values may result from the thermal boundary conditions used in the theory or numerical simulation where the average temperatures or temperature difference were obtained from the measured tube surface temperatures at the first two and the last two columns of the tube bundles. This was found to achieve the better agreement with the experimental

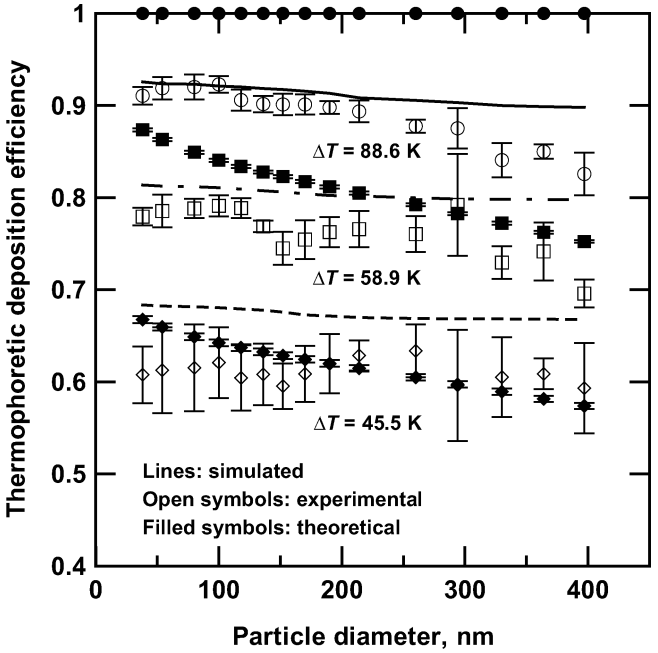

FIG. 9. Comparison of the simulated, experimental, and theoretical thermophoretic deposition efficiency at three temperature differences. Inlet air flow temperature: 298 K, flow rate: 0.6 L/min.

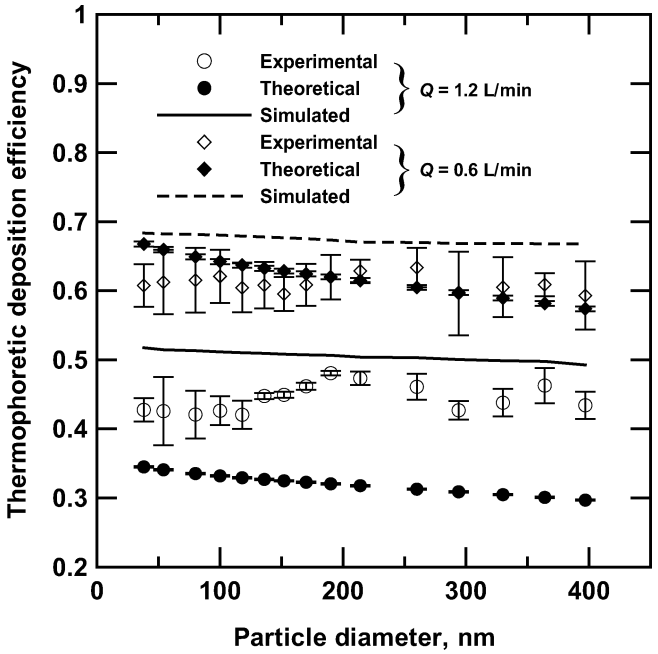

FIG. 10. Comparison of the experimental, simulated, and theoretical thermophoretic deposition efficiency when the hot silicon oil temperature is 423 K at the flow rate of 0.6 and 1.2 L/min, respectively.

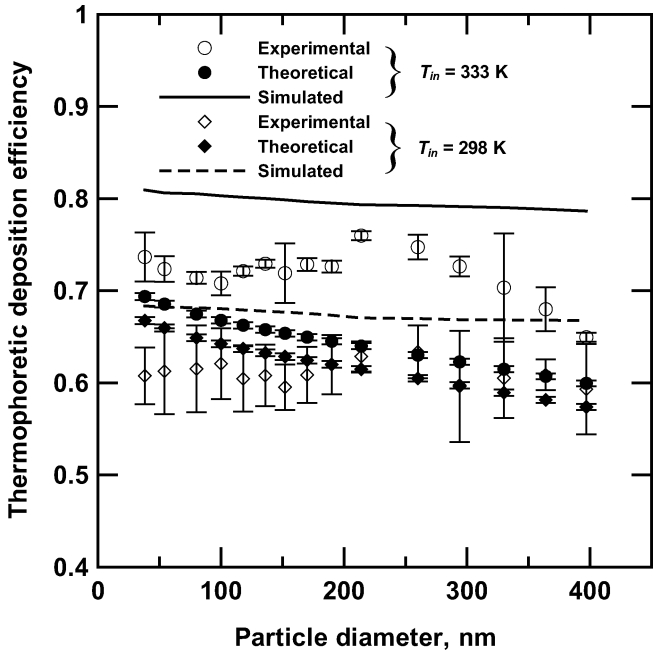

FIG. 11. Effect of inlet temperature of the aerosol flow on the thermophoretic deposition efficiency when the flow rate is 0.6 L/min.

thermophoretic deposition efficiency data while using the geometric mean temperature or temperature difference in the theory or numerical simulation was found to lead to larger deviation.

The thermophoretic precipitator was tested at two aerosol flow rates of 0.6 and 1.2 L/min, respectively. Figure 10 shows the comparison of the experimental, simulated and theoretical thermophoretic deposition efficiencies when the hot silicon oil temperature is 423 K at the flow rate of 0.6 and 1.2 L/min, respectively. The experimental thermophoretic deposition efficiency is reduced from 59.3–63.4% to 42–48% when the flow rate is increased from 0.6 to 1.2 L/min. The deviation of the present simulation and theoretical prediction from the experimental data are found to be 2.6–9.3% and 8.3–16.2%, respectively, at the flow rate of 1.2 L/min. The thermophoretic deposition efficiencies are seen to reduce with the increasing aerosol flow rate from 0.6 to 1.2 L/min.

Figure 11 shows the effect of inlet temperature of the aerosol flow on the thermophoretic deposition efficiency. The experimental thermophoretic deposition efficiency increases from 59.3–63.4% to 64.9–76% when the inlet air flow temperature is increased from 298 to 333 K at the flow rate of 0.6 L/min. The deviation of the present simulation and theoretical prediction from the experimental data are found to be 3.4–13.7% and 3.8–12%, respectively, when the inlet air flow temperature is 333 K at the flow rate of 0.6 L/min. Results show that increasing inlet air flow temperature will increase the deposition efficiency.

In Figures 9 to 11, thermophoretic deposition efficiencies are seen to remain nearly constant with respect to particle size. In addition, the thermophoretic deposition efficiency increases as the temperature gradient is increased or particle size is decreased, which all agree with the theoretical expression of the thermophoretic deposition efficiency.

According to Equation (6), the thermophoretic deposition efficiency can be expressed as a linear function of the dimensionless precipitator number, $(L\mu_{g,0}\Delta T)/(\rho_{g,0}v_{x,0}H^2T)$, which

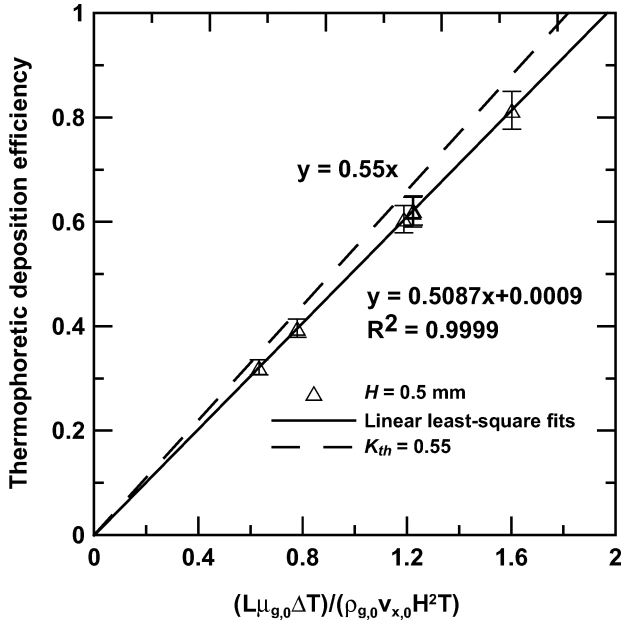

FIG. 12. Theoretical thermophoretic deposition efficiency plotted against the dimensionless precipitator number, $(L\mu_{g,0}\Delta T)/(\rho_{g,0}v_{x,0}H^2T)$.

was first discussed by Messerer et al. (2003) then followed by Messerer et al. (2004). Figure 12 shows the theoretical thermophoretic deposition efficiency plotted against the dimensionless precipitator number. The lines are linear least-square fit to the data sets (solid) and the theoretical relationship for the plate-to-plate thermophoretic precipitator (dashed). The slope of the fit line is close to the constant value of $K_{th} = 0.55$ derived by Waldmann and Schmitt (1966) in the free molecular regime. Results suggest that the theoretical formula derived from the plate-to-plate thermophoretic precipitator, which is suitable for predicting the thermophoretic deposition efficiency as a function of thermal and flow conditions, can be used to design and scale-up of the present thermophoretic precipitator.

CONCLUSION

A new cross-flow tube bundle heat exchanger has been designed and tested for thermophoretic deposition of submicron aerosol particles. The present design has five columns of hot and cold square tubes, respectively, arranged in a staggered manner to maintain a nearly constant temperature gradient in the direction of the aerosol flow. The thermophoretic precipitator is capable of removing submicron particles efficiently to overcome the shortcomings of drastic reduction of temperature gradient and deposition efficiency in the conventional designs. Experimental results show that the present thermophoretic precipitator has good particle deposition efficiency up to 92% for the aerosol flow at room temperature. Numerical simulation was further conducted to validate the experimental data and good agreement was obtained. The empirical equation of the plate-to-plate thermophoretic precipitator derived by Tsai and Lu (1995) was shown to be suitable for predicting the theoretical thermophoretic deposition efficiency to facilitate the design and scale-up of the present precipitator.

The present design can maintain high temperature gradient throughout the entire precipitator and the gap between the cold and hot square tubes can be adjusted easily. The aerosol flow rate can be increased further as the number of hot and cold tubes can be increased easily. It can be used as the control device for the control of the diesel engine and other high temperature exhaust gases, or used as the indoor air cleaner. The present design is best suited when it is also used as a heat exchanger to recover thermal energy while maintaining a high temperature gradient for thermophoretic particle precipitation. However, it is necessary to coat the deposition surfaces with oxidizing catalyst to burn off the collected particles, or use purging air flow to clean the surfaces regularly to prevent particle clogging inside the precipitator.

NOMENCLATURE

C = slip correction factor (dimensionless)
C_m = momentum exchange coefficient (dimensionless)
C_s = thermal slip coefficient (dimensionless)
C_t = temperature jump coefficient (dimensionless)
D = particle diffusivity (m^2/s)
H = plate distance (m)
k_g = gas thermal conductivity (W/m K)
k_p = particle thermal conductivity (W/m K)
K_{th} = thermophoretic coefficient (dimensionless)
L = deposition length (m)
N = particle concentration (particles/m^3)
N_i = particle concentration at inlet (particles/m^3)
N_o = particle concentration at outlet (particles/m^3)
Q = volumetric flow rate (L/min)
T = temperature (K)
T_{cold} = cold water temperature (K)
T_{hot} = hot silicon oil temperature (K)
T_{in} = inlet air temperature (K)
T_{out} = outlet air temperature (K)
ΔT = temperature difference (K)
$\vec{\nabla} T$ = temperature gradient (K/m)
$\bar{u}$ = gas velocity (m/s)
$\bar{V}_{th}$ = thermophoretic velocity (m/s)
$v_{x,0}$ = average axial velocity (m/s)

Greek letters

η = deposition efficiency
η_{iso} = isothermal deposition efficiecny
η_{th} = thermophoretic deposition efficiency
η_{tot} = total deposition efficiency
λ = mean free path of air molecules (m)
μ_g = gas dynamic viscosity (kg/ms)
ν = kinematic viscosity (N s/m^2)
ρ_g = gas density (kg/m^3)

Additional subscripts

0 = arithmetic mean value

REFERENCES

Bang, J. J., Trillo, E. A., and Murr, L. E. (2003). Utilization of Selected Area Electron Diffraction Patterns for Characterization of Air Submicron Particulate Matter Collected by a Thermophoretic Precipitator, *J. Air Waste Manage.* 53:227–236.

Batchelor, G. K., and Shen, C. (1985). Thermophoretic Deposition of Particles in Gas Flowing over Cold Surfaces, *J. Colloid Interf. Sci.* 107:21–37.

Chang, Y. C., Ranade, M. B., and Gentry, J. W. (1995). Thermophoretic Deposition in Flow along an Annular Cross Section: Experiment and Simulation, *J. Aerosol Sci.* 26:407–428.

El-Shaboury, A. M. F., and Ormiston, S. J. (2005). Analysis of Laminar Forced Convection of Air Crossflow in In-line Tube Banks with Nonsquare Arrangements, *Numer. Heat Tran. A-Appl.* 48:99–126.

Gonzalez, D., Nasibulin, A. G., Baklanov, A. M., Shandakov, S. D., Brown, D. P., Queipo, P., and Kauppinen, E. I. (2005). A New Thermophoretic Precipitator for Collection of Nanometer-Sized Aerosol Particles, *Aerosol Sci. Technol.* 39:1064–1071.

He, C., and Ahmadi, G. (1998). Particle Deposition with Thermophoresis in Laminar and Turbulent Duct Flows, *Aerosol Sci. Technol.* 29:525–546.

Hinds, W. C. (1999). *Aerosol Technology*, John Wiley & Sons, New York.

Housiadas, C., Mueller, K., Carlsson, J., and Drossinos, Y. (2001). Two Dimensional Effects in Thermophoretic Particle Deposition: The Phebus-FP Steam Generator. European Aerosol Conference, Leipzig, *J. Aerosol Sci*. 32(Suppl. 1):S1029–S1030.

Housiadas, C., and Drossinos, Y. (2003). Thermophoretic Deposition of Low-inertia Particles. European Aerosol Conference, Madrid, *J. Aerosol Sci.* 34(Suppl. 1):S113–S114.

Housiadas, C., and Drossinos, Y. (2005). Thermophoretic Deposition in Tube Flow, *Aerosol Sci. Technol.* 39:304–318.

Incropera, F. P., and DeWitt, D. P. (2002). *Fundamentals of Heat and Mass Transfer*, John Wiley & Sons, New York.

Khan, W. A., Culham, J. R., and Yovanovich, M. M. (2006). Convection Heat Transfer from Tube Banks in Crossflow: Analytical Approach, *Int. J. Heat Mass Tran.* 49:4831–4838.

Lee, B. U., Byun, D. S., Bae, G. N., and Lee, J. H. (2006). Thermophoretic Deposition of Ultrafine Particles in a Turbulent Pipe Flow: Simulation of Ultrafine Particle Behaviour in an Automobile Exhaust Pipe, *J. Aerosol Sci.* 37:1788–1796.

Lin, J.-S., and Tsai, C.-J. (2003). Thermophoretic Deposition Efficiency in a Cylindrical Tube Taking into Account Developing Flow at the Entrance Region, *J. Aerosol Sci.* 34:569–583.

Lin, J.-S., Tsai, C.-J., and Chang, C.-P. (2004). Suppression of Particle Deposition in Tube Flow by Thermophoresis, *J. Aerosol Sci.* 35:1235–1250.

Lin, J.-S., Tsai, C.-J., Tung K.-L., and Chiang, H.-C. (2008). Thermophoretic Particle Deposition Efficiency in Turbulent Tube Flow, *J. Chin. Inst. Chem. Eng.* 39:281–285.

Lorenzo, R., Kaegi, R., Gehrig, R., Scherrer, L., Grobety, B., and Burtscher, H. (2007). A Thermophoretic Precipitator for the Representative Collection of Atmospheric Ultrafine Particles for Microscopic Analysis, *Aerosol Sci. Technol.* 41:934–943.

Maynard, A. D. (1995). The Development of a New Thermophoretic Precipitator for Scanning-Transmission Electron-Microscope Analysis of Ultrafine Aerosol-Particles, *Aerosol Sci. Technol.* 23:521–533.

Messerer, A., Niessner, R., and Poschl, U. (2003). Thermophoretic Deposition of Soot Aerosol Particles under Experimental Conditions Relevant for Modern Diesel Engine Exhaust Gas Systems, *J. Aerosol Sci.* 34:1009–1021.

Messerer, A., Niessner, R., and Poschl, U. (2004). Miniature Pipe Bundle Heat Exchanger for Thermophoretic Deposition of Ultrafine Soot Aerosol Particles at High Flow Velocities, *Aerosol Sci. Technol.* 38:456–466.

Messerer, A., Schmatloch, V., Poeschl, U., and Niessner, R. (2007). Combined Particle Emission Reduction and Heat Recovery from Combustion Exhaust—A Novel Approach for Small Wood-Fired Appliances, *Biomass Bioenerg.* 31:512–521.

Montassier, N., Boulaud, D., Stratmann, F., and Fissan, H. (1990). Comparison between Experimental Study and Theoretical Model of Thermophoretic Particle Deposition in Laminar Tube Flow, *J. Aerosol Sci.* 21:S85–S88.

Montassier, N., Boulaud, D., and Renoux, A. (1991). Experimental Study of Thermophoretic Particle Deposition in Laminar Tube Flow, *J. Aerosol Sci.* 22:677–687.

Munoz-Bueno, R., Hontanon, E., and Rucandio, M. I. (2005). Deposition of Fine Aerosols in Laminar Tube Flow at High Temperature with Large Gas-to-Wall Temperature Gradients, *J. Aerosol Sci.* 36:495–520.

Patankar, S. V. (1980). *Numerical Heat Transfer and Fluid Flow*, Hemisphere, Washington, D. C.

Pyykönen, J., and Jokiniemi, J. (2000). Computational Fluid Dynamics Based Sectional Aerosol Modelling Schemes, *J. Aerosol Sci.* 31:531–550.

Romay, F. J., Takagaki, S. S., Pui, D. Y. H., and Liu, B. Y. H. (1998). Thermophoretic Deposition of Aerosol Particles in Turbulent Pipe Flow, *J. Aerosol Sci.* 29:943–959.

Shi, J. P., and Harrison, R. M. (2001). Study of a Water-Colded Fluidized Bed for Diesel Particle Agglomeration, *Powder Technol.* 115:146–156.

Stratmann, F., and Whitby, E. R., (1989). Numerical-Solution of Aerosol Dynamics for Simultaneous Convection, Diffusion and External Forces, *J. Aerosol Sci.* 20:437–440.

Stratmann, F., Otto, E., and Fissan, H. (1994). Thermophoretic and Diffusional Particle Transport in Colded Laminar Tube Flow, *J. Aerosol Sci.* 25:1305–1319.

Talbot, L., Cheng, R. K., Schefer, R. W., and Willis, D. R. (1980). Thermophoresis of Particles in a Heated Boundary Layer, *J. Fluid Mech.* 101:737–758.

Tsai, C.-J., and Lu, H.-C. (1995). Design and Evaluation of a Plate-to-Plate Thermophoretic Precipitator, *Aerosol Sci. Technol.* 22:172–178.

Tsai, C.-J., Lin, J.-S., Aggarwal, S. G., and Chen, D.-R. (2004). Thermophoretic Deposition of Particles in Laminar and Turbulent Tube Flows, *Aerosol Sci. Technol.* 22:172–180.

Waldmann, L. Z., and Schmitt, K. H. (1966). Thermophoresis and Diffusiophoresis of Aerosols, in *Aerosol Science*, C. N. Davis, ed., London: Academic Press.

Wang, Y. Q., Penner, L. A., and Ormiston, S. J. (2000). Analysis of Laminar Forced Convection of Air for Crossflow in Banks of Staggered Tubes, *Numer. Heat Tr. A-Appl.* 38:819–845.

Wen, J., and Wexler, A. S. (2007). Thermophoretic Sampler and Its Application in Ultrafine Particle Collection, *Aerosol Sci. Technol.* 41:624–629.